JACS
JOURNAL OF THE AMERICAN CHEMICAL SOCIETY

COMMUNICATION

pubs.acs.org/JACS

Reaction-Driven Surface Restructuring and Selectivity Control in Allylic Alcohol Catalytic Aerobic Oxidation over Pd

Adam F. Lee,*[,†] Christine V. Ellis,[†] James N. Naughton,[‡] Mark A. Newton,[§] Christopher M. A. Parlett,[†] and Karen Wilson[†]

[†]Cardiff Catalysis Institute, School of Chemistry, Cardiff University, Cardiff CF10 3AT, U.K.

[‡]Department of Physics, University of York, York YO10 5DD, U.K.

[§]European Synchrotron Radiation Facility, 6 Rue Jules Horowitz, BP-220, F-38043 Grenoble, France

Supporting Information

ABSTRACT: Synchronous, time-resolved DRIFTS/MS/XAS cycling studies of the vapor-phase selective aerobic oxidation of crotyl alcohol over nanoparticulate Pd have revealed surface oxide as the desired catalytically active phase, with dynamic, reaction-induced Pd redox processes controlling selective versus combustion pathways.

There has been much recent interest in the development of heterogeneously catalyzed, aerobic selective oxidation (selox) routes to transform diverse primary alcohols to aldehydes.[1−3] Allylic aldehydes are valuable intermediates for the fine chemical, pharmaceutical, and agrochemical sectors. For example, crotyl alcohol (CrOH) is an important agrochemical and precursor to the food preservative sorbic acid, while cinnamaldehyde confers a cinnamon aroma. The commercial synthesis of allylic aldehydes often proceeds via oxidation of their alcohol analogues by hazardous stoichiometric oxidants. In addition to safety considerations, such current technologies are also atom-inefficient because of poor selectivity and/or additional separation and waste treatment steps to isolate the product and therefore economically disadvantageous.[4] Solid catalysts able to utilize O_2 can circumvent these limitations to afford alternative continuous aerobic selox processes.[5] The most promising of such heterogeneous catalysts derive from nanocrystalline Au[6] and Pd[7,8] and bimetallic formulations thereof,[9] typically dispersed on high-area carbon[10] or oxide supports.[9,11] Despite these advances, future catalyst design and optimization is hampered by our limited understanding of the active site responsible for the (rate-limiting) oxidative dehydrogenation step[12,13] and its associated response to reaction conditions.

Early mechanistic studies aimed at elucidating the active site in alcohol selox by platinum-group metals (PGMs) were compromised by the use of corrosive electrolytes[1] and/or strongly adsorbing surfactants, which are now known to influence the oxidation state and morphology.[14] Subsequent in situ, liquid-phase extended X-ray absorption fine structure (EXAFS) spectroscopy investigations identified important on-stream changes in the oxidation state of supported Pd clusters during alcohol oxidations. In the first dynamic quick EXAFS study of a solid catalyst during a liquid-phase reaction,[15] we reported a correlation between PdO content and crotyl and cinnamyl alcohol selox rates, while the converse was noted[16] for benzyl alcohol selox. Unfortunately, the complexities of these three-phase studies make it impossible to eliminate mass-transport limitations or competitive solvent adsorption and to achieve accurate control over the oxygen versus alcohol concentrations during the reaction. Similar provisos apply to complementary ATR-IR measurements,[17] wherein reactively formed CO and benzoate accumulated at the surface of Pd catalysts under reducing environments. Pre- and in situ[15] reduction protocols both suppress crotyl and cinnamyl alcohol selox over PGMs. Time-resolved X-ray photoelectron spectroscopy (XPS)[18] and thermal desorption[19] studies over model Pd catalysts showed that metallic (111) facets promote crotonaldehyde decarbonylation and implied an important role for coadsorbed oxygen in ameliorating such self-poisoning. Indeed, we recently postulated a direct relationship between Pd^{2+} surface (and bulk) concentrations determined ex situ and the associated turnover frequency toward crotyl, benzyl, and cinnamyl alcohol selox.[8]

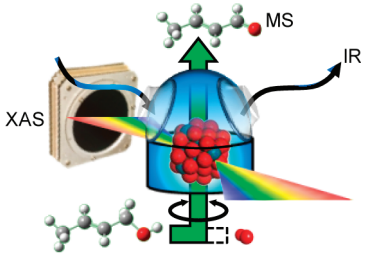

Figure 1. Synchronous DRIFTS/MS/XAS measurements were recorded in a stainless steel reactor with vitreous carbon windows that permit high X-ray transmission with minimum interference to the XAS signal.[21] Heated inlet and outlet gas lines prevent condensation of less-volatile components.

Here we utilized the powerful combination of energy-dispersive X-ray absorption spectroscopy (XAS), diffuse-reflectance Fourier transform IR spectroscopy (DRIFTS), and online mass spectrometry (MS)[20] in a dynamic in situ study of the vapor-phase selox of CrOH ($CH_3CH{=}CH{-}CH_2OH$) over diverse nanoparticulate Pd catalysts that are active toward this reaction in the liquid phase.[8] Crucially, by working in the vapor phase, we were able to minimize artifacts arising from diffusion limitations or solvent effects common in liquid-phase selox and interrogate the nature of adsorbates present on the surface of the catalyst (DRIFTS) and any associated restructuring (XAS) while monitoring the global reactivity via the gaseous exhaust stream composition with 1 Hz time resolution. Adoption of a *transient* approach enabled us to delineate quantitative structure−function

Received: January 24, 2011
Published: March 25, 2011

   dx.doi.org/10.1021/ja200684f | J. Am. Chem. Soc. 2011, 133, 5724–5727

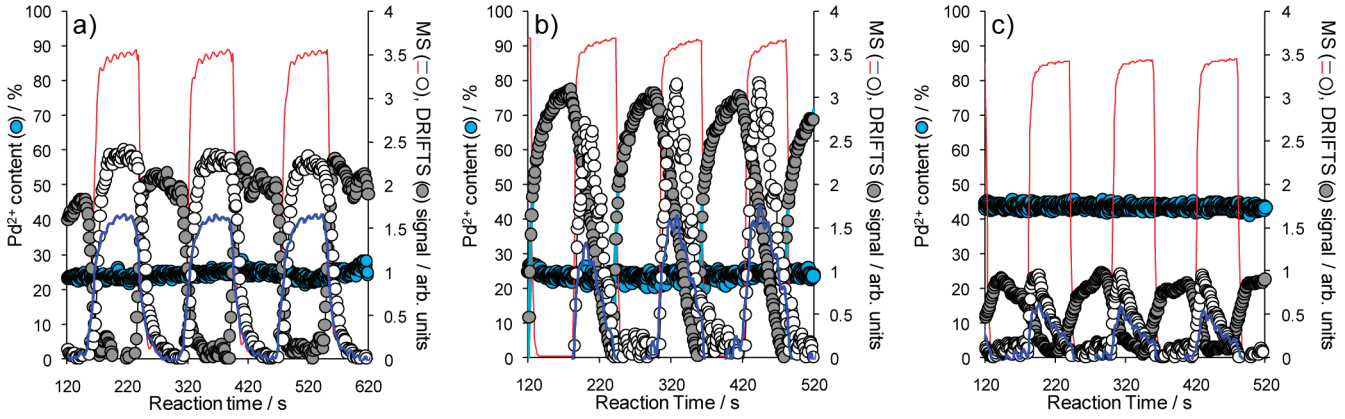

Figure 2. DRIFTS/MS/XANES intensities as a function of alternating CrOH/O_2 cycles over (a) 2.37 wt % Pd/mesoporous Al_2O_3, (b) 2.5 wt % Pd/SBA-15, and (c) Pd nanoicosahedra/mesoporous Al_2O_3 at 80 °C: gray ●, 1712 cm^{-1} $\nu_{C=O}$; blue line, H_2O (m/z 18); red line, O_2 (m/z 32); ○, crotonaldehyde (m/z 70); blue ●, fitted XANES Pd^{2+} concentration.

relations on a dispersed catalyst with a precision never previously achieved via conventional steady-state liquid- or vapor-phase measurements for any heterogeneously catalyzed organic transformation. We have unequivocally demonstrated that low temperatures stabilize partially oxidized Pd clusters that are selective for the production and release of reactively formed crotonaldehyde, while >150 °C catalyst reduction promotes combustion.

Figure 1 illustrates the in situ reaction cell developed for simultaneous energy-dispersed DRIFTS/MS/XAS measurements.[21] Alternating cycles of CrOH (in He) or O_2 (in He) were passed over three distinct as-prepared catalysts while maintaining an isothermal bed temperature: 2.37 wt % Pd/mesoporous Al_2O_3 and 2.2 wt % Pd/SBA-15 prepared via incipient wetness impregnation and and a 5 wt % poly(vinylpyrrolidone) (PVP)-stabilized Pd nanoicosahedra sol immobilized on mesoporous Al_2O_3. These experiments were repeated between 80 and 250 °C (CrOH could not be maintained in the vapor phase at lower temperatures).

The resulting low-temperature catalyst behavior is shown in Figure 2, which compares X-ray absorption near-edge structure (XANES) analysis of the time-dependent Pd K-edge XAS spectra with the principal surface and evolved gas-phase products detected by DRIFTS and MS, respectively. Only the integrated O_2 reactant MS signal (m/z 32) is shown; the alternating CrOH reactant (m/z 72) has been omitted for clarity. Rapid and reproducible switching of the reactant feedstream was achieved, with adsorbate and effluent concentrations equilibrating in under 12 s.

The first important observation is that the palladium oxidation state remained unperturbed throughout the cycling experiments irrespective of the Pd catalyst, fitting to partially oxidized phases (containing ∼20−40% total PdO) characteristic of the fresh catalysts. There was also good agreement between the corresponding fitted EXAFS spectra (Figure S8 in the Supporting Information), evidencing high stability under the cycled redox environments at 80 °C. It is important to note that while XAS is an averaging technique, Pd oxidation is a surface reaction rate-limited process,[22] so oxide features are dominated by the selvage of our nanoparticles. MS data show that the only reactively formed products desorbed from all three catalyst surfaces at any temperature were crotonaldehyde and water, CO/propene, and CO_2, indicative of oxidative dehydrogenation, decarbonylation, and combustion pathways, respectively. Product desorption was negligible under CrOH cycles at 80 °C, but the switchover to gas-phase O_2 triggered the rapid release of water and crotonaldehyde (Figure 2, m/z 18 and 70), precisely as expected from oxidative dehydrogenation, accompanied by trace CO and propene (omitted for clarity). The temporal evolution of all four products closely mirrored that of the oxygen reactant for each catalyst, with a return to gas-phase CrOH almost instantaneously suppressing their liberation from the catalyst surface.

The synchronous DRIFTS spectra show that exposure of the impregnated and sol-immobilized catalysts to gas-phase CrOH immediately induced surface vibrational modes characteristic of both the alcohol reactant and crotonaldehyde (Figure S13). The concentration of reactively formed crotonaldehyde on the catalyst surfaces was monitored by its associated 1712 cm^{-1} band ($\nu_{C=O}$). A striking antiphase pattern between crotonaldehyde production and surface confinement during CrOH cycles and subsequent liberation of this desired selox product into the gas phase upon switching to an O_2 stream is apparent. This observation is precisely in accordance with our recent single-crystal investigations of CrOH selox, wherein coadsorbed oxygen adatoms promoted crotonaldehyde desorption from Pd surfaces, thereby suppressing secondary reactions.[19] There was no evidence of maleic anhydride or crotonic acid under these conditions. We should also note the presence of weak features at 1915 and 2035 cm^{-1} for the 2.37 wt % Pd/mesoporous Al_2O_3 sample, which we assign to molecular CO bound at metallic Pd bridge and atop sites, respectively. The extinction coefficient of linearly bound CO is orders of magnitude greater than the carbonyl stretch in propionaldehyde or $\nu_{C=C}$ of allyl alcohol (4.95 vs 0.4 vs 0.026 mL mg^{-1} mm^{-1}),[23] so this CO coverage represents only a few percent of the adsorbed oxygenate. Surface Pd−H could not be detected, but requires H_2 pressures >9 Torr,[24] exceeding that generated in situ from CrOH. It is important to note the qualitatively similar behavior of our three catalysts, independent of the support or mode of Pd nanoparticle genesis, evidencing a common reaction mechanism and active site.

The system behavior changed dramatically above 180 °C, with both the catalyst structure and reaction products evidencing different surface−adsorbate chemistry. XANES showed the Pd oxidation state for all three catalysts to exhibit a dynamic response to the external reactant environment, falling to ∼10−27% Pd^{2+} under the reducing CrOH/He stream and rapidly reoxidizing to ∼28−50% Pd^{2+} upon switching to the O_2/He stream (Figure 3a and Figure S5a,b). Normalized spectra are shown in Figure S6 for the 2.37 wt % Pd/mesoporous Al_2O_3 catalyst, with the associated EXAFS fits in Table S1 and Figure S8. Although the magnitude of these oxidation-state changes depended on the Pd catalyst, the time/reactant dependence was invariant, highlighting a phenomenon general to Pd. This reactant-induced surface restructuring was

dx.doi.org/10.1021/ja200684f |J. Am. Chem. Soc. 2011, 133, 5724–5727

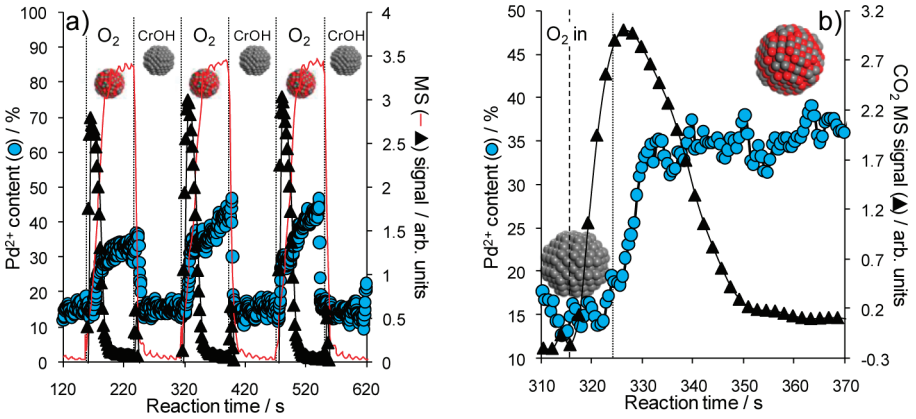

Figure 3. (a) MS/XANES intensities during alternating CrOH/O_2 cycles over the 2.37 wt % Pd/mesoporous Al_2O_3 catalyst at 250 °C: red line, O_2 (m/z 32); ▲, CO_2 (m/z 44); blue ●, fitted XANES Pd^{2+} concentration. (b) Evolution of CO_2 yield and Pd oxidation state during CrOH/He → O_2/He switchover of the reactant stream over the 2.37 wt % Pd/mesoporous Al_2O_3 catalyst at 250 °C. Combustion occurs before reoxidation of metal nanoparticles.

fully reversible and accompanied by a switchover from selective to total oxidation with increasing temperature (see below). While the latter is anticipated on simple thermodynamic grounds, the temporal evolution of products revealed unexpected features of this high-temperature chemistry. The transition from an oxidizing to a reducing environment (and consequently a PdO_x to Pd catalyst) occurred in less than 2 s as gas-phase O_2 mixed with CrOH before being swept from the system. Only weak, coincident CO_2 pulses were observed, indicating that PdO_x surfaces are almost inactive for CrOH combustion. Lattice/surface oxygen extracted from the catalysts during this PdO_x → Pd transformation was predominantly consumed through oxidative dehydrogenation (see the next paragraph). In contrast, subsequent exposure of reduced (hydrocarbon-saturated) Pd surfaces to gas-phase O_2 produced an instantaneous, intense CO_2 burst (Figure 3b), evidencing accumulation of significant carbonaceous CH_x residues over metallic Pd nanoparticles. Combustion was followed by slower Pd reoxidation, the latter continuing throughout the oxidizing cycle. Nanoparticle sizes were temperature-invariant for all three catalysts (Table S1 and Figures S7 and S9), evidencing negligible sintering.

The question of the fate of oxygen lost from the catalysts during the O_2/He → CrOH/He switchover arises. Figure 4 shows corresponding reaction profiles for the minor selective and partial oxidation products over the 2.37 wt % Pd/mesoporous Al_2O_3 catalyst (Figure S5b,c reveals similar behavior for the other catalysts). It is evident that in the absence of gas-phase O_2, PdO_x is active for the oxidative dehydrogenation of CrOH to crotonaldehyde via rapid abstraction of lattice/surface oxygen adatoms. However, only a fraction of this reactively formed aldehyde desorbs intact, since this selox step is accompanied by the genesis of metallic Pd sites that in turn catalyze decarbonylation and concomitant evolution of CO and C_3H_6 into the gas phase.[19] The relative selox performance of Pd versus PdO_x nanoparticles can be directly estimated from the integrated crotonaldehyde desorption signals during their respective reducing/oxidizing cycles; *66% more gas-phase crotonaldehyde is liberated from nanoparticulate PdO_x than from the metal.*

There are two limiting scenarios to explain the partial catalyst reduction/oxidation observed at high temperature: either the as-prepared catalysts contained inhomogeneous distributions of discrete small oxidic and large metallic Pd nanoparticles and the reactant feedstock influenced their relative populations, or the observed redox behavior reflects the reversible genesis of oxide shells encapsulating metal cores uniformly across every nanoparticle in each catalyst.

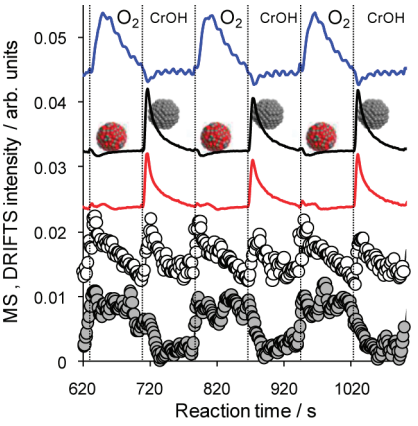

Figure 4. DRIFTS/MS intensities during alternating CrOH/O_2 cycles over the 2.37 wt % Pd/mesoporous Al_2O_3 catalyst at 250 °C showing higher crotonaldehyde (and crotonic acid) formation over PdO_x than over Pd: blue line, H_2O (m/z 18); black line, C_3H_6 (m/z 41); red line, CO (m/z 28); ○, crotonaldehyde (m/z 70); gray ●, crotonic acid 1720 cm^{-1}.

Transmission electron microscopy (TEM) and X-ray diffraction provided no evidence of the former. If the latter scenario were true, then the degree of oxidation should be proportional to the surface: bulk Pd atom ratio (dispersion) of particles, with formation of a two-dimensional PdO_x capping layer passivating further oxidation of the underlying Pd. We estimated the Pd dispersion of fresh nanoparticles in our 2.37 wt % Pd/mesoporous Al_2O_3 catalyst to be 47% by CO chemisorption and TEM, in accordance with geometric predictions for an unrelaxed 2.3 nm cuboctahedral particle (204 surface vs 429 bulk atoms). This value is indeed close to the 44% maximum PdO observed in Figure 3a. In-situ XPS (Figures S10−S12) confirmed reduction of surface PdO_x upon CrOH adsorption at 250 °C.

The temperature-dependent transition from selective CrOH oxidation to combustion was quantified for the 2.37 wt % Pd/mesoporous Al_2O_3 catalyst (Figure 5). At low conversion (low T), crotonaldehyde was the dominant product via oxidative dehydrogenation (the predicted oxygen consumption for this sole pathway is indicated in green). Above 150 °C, alcohol and oxygen conversion rose rapidly, the latter reflecting the emergence of total oxidation pathways, which in turn dominated by 250 °C (the predicted O_2 consumption for combustion is indicated in red). Together, these experiments provide direct evidence of a generic

dx.doi.org/10.1021/ja200684f |*J. Am. Chem. Soc.* 2011, 133, 5724–5727

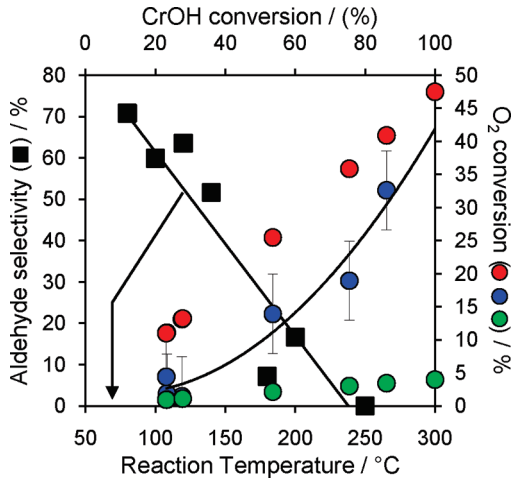

Figure 5. Switchover from selective to partial CrOH oxidation to combustion with increasing temperature (conversion). Predicted relationships between CrOH and O_2 conversion for selective oxidative dehydrogenation (green ●) and total combustion (red ●) are also shown.

Scheme 1. Proposed Reaction Network Interrelating Nanoparticulate Catalyst Phase (Oxidation State) and Associated Selectivity toward CrOH Oxidation upon the Surrounding Reducing or Oxidizing Reactant Feedstream

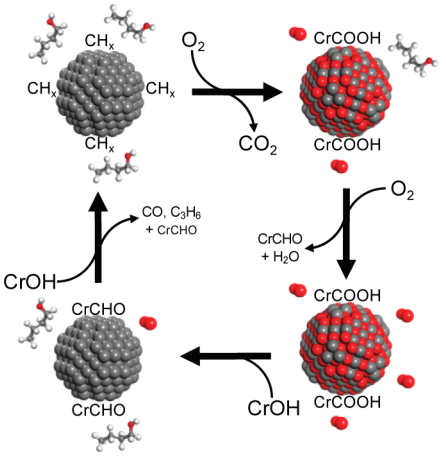

mechanism for Pd-catalyzed selox wherein metallic Pd nanoparticles favor CrOH decarbonylation and combustion pathways while Pd^{2+} favors oxidative dehydrogenation to crotonaldehyde at low temperature, with oxygen insertion to form surface-bound crotonic acid competing at high temperature. The interdependence of the reactant environment, catalyst oxidation state, and surface chemistry above 150 °C is shown in Scheme 1.

We have demonstrated the first application of time-resolved synchrotron X-ray absorption spectroscopy to simultaneously follow dynamic nanoparticle surface restructuring and the evolution of surface and gas-phase products during an organic reaction. Surface PdO_x, not Pd, has been identified as the catalytic species responsible for the selective oxidation of CrOH to crotonaldehyde. Elevated reaction temperatures facilitate reversible nanoparticle redox processes and concomitant catalytic selectivity loss in response to reaction conditions. These discoveries highlight the importance of stabilizing surface PdO_x and minimizing catalyst reducibility in order to achieve high selox yields and will hopefully aid the future design of Pd-derived selox catalysts. The utility of combined DRIFTS/MS/XAS measurements for probing complex reaction networks also paves the way for related vapor-phase fine-chemicals catalysis studies within this milieu.

■ ASSOCIATED CONTENT

Supporting Information. Catalyst synthesis, characterization and reaction conditions. This material is available free of charge via the Internet at http://pubs.acs.org.

■ AUTHOR INFORMATION

Corresponding Author
leeaf@cardiff.ac.uk

■ ACKNOWLEDGMENT

We thank the EPSRC (EP/E046754/1, EP/G007594/2) for financial support, a Leadership Fellowship (A.F.L.), and studentship support (C.V.E., J.N.N., and C.M.A.P.) and the ESRF for beamtime (CH2432). A.F.L. thanks Miss Carly J. Broderick for invaluable support.

■ REFERENCES

(1) Mallat, T.; Baiker, A. *Chem. Rev.* **2004**, *104*, 3037.
(2) Meenakshisundaram, S.; Nowicka, E.; Miedziak, P. J.; Brett, G. L.; Jenkins, R. L.; Dimitratos, N.; Taylor, S. H.; Knight, D. W.; Bethell, D.; Hutchings, G. J. *Faraday Discuss.* **2010**, *145*, 341.
(3) Vinod, C. P.; Wilson, K.; Lee, A. F. *J. Chem. Technol. Biotechnol.* **2011**, *86*, 161.
(4) ten Brink, G. J.; Arends, I.; Sheldon, R. A. *Science* **2000**, *287*, 1636.
(5) Sheldon, R. A.; Arends, I.; Hanefeld, U. In *Green Chemistry and Catalysis*; Wiley-VCH: Weinheim, Germany, 2007.
(6) Della Pina, C.; Falletta, E.; Prati, L.; Rossi, M. *Chem. Soc. Rev.* **2008**, *37*, 2077.
(7) Mori, K.; Hara, T.; Mizugaki, T.; Ebitani, K.; Kaneda, K. *J. Am. Chem. Soc.* **2004**, *126*, 10657.
(8) Hackett, S. E. J.; Brydson, R. M.; Gass, M. H.; Harvey, I.; Newman, A. D.; Wilson, K.; Lee, A. F. *Angew. Chem., Int. Ed.* **2007**, *46*, 8593.
(9) Enache, D. I.; Edwards, J. K.; Landon, P.; Solsona-Espriu, B.; Carley, A. F.; Herzing, A. A.; Watanabe, M.; Kiely, C. J.; Knight, D. W.; Hutchings, G. J. *Science* **2006**, *311*, 362.
(10) Bianchi, C. L.; Biella, S.; Gervasini, A.; Prati, L.; Rossi, M. *Catal. Lett.* **2003**, *85*, 91.
(11) Li, C. L.; Zhang, Q. H.; Wang, Y.; Wan, H. L. *Catal. Lett.* **2008**, *120*, 126.
(12) Lee, A. F.; Hackett, S. F. J.; Hargreaves, J. S. J.; Wilson, K. *Green Chem.* **2006**, *8*, 549.
(13) Grunwaldt, J. D.; Caravati, M.; Baiker, A. *J. Phys. Chem. B* **2006**, *110*, 25586.
(14) Lee, A. F.; Wilson, K.; Lambert, R. M.; Hubbard, C. P.; Hurley, R. G.; McCabe, R. W.; Gandhi, H. S. *J. Catal.* **1999**, *184*, 491.
(15) Lee, A. F.; Wilson, K. *Green Chem.* **2004**, *6*, 37.
(16) Keresszegi, C.; Ferri, D.; Mallat, T.; Baiker, A. *J. Phys. Chem. B* **2005**, *109*, 958.
(17) Ferri, D.; Mondelli, C.; Krumeich, F.; Baiker, A. *J. Phys. Chem. B* **2006**, *110*, 22982.
(18) Lee, A. F.; Chang, Z.; Ellis, P.; Hackett, S. F. J.; Wilson, K. *J. Phys. Chem. C* **2007**, *111*, 18844.
(19) Naughton, J.; Lee, A. F.; Thompson, S.; Vinod, C. P.; Wilson, K. *Phys. Chem. Chem. Phys.* **2010**, *12*, 2670.
(20) Newton, M. A.; Belver-Coldeira, C.; Martinez-Arias, A.; Fernandez-Garcia, M. *Nat. Mater.* **2007**, *6*, 528.
(21) Newton, M. A. *Top. Catal.* **2009**, *52*, 1410.
(22) Salmeron, M.; Schlogl, R. *Surf. Sci. Rep.* **2008**, *63*, 169.
(23) Chong, T. S.; Tan, S. T.; Fan, W. Y. *Chem.—Eur. J.* **2006**, *12*, 5128.
(24) Ratajczykowa, I. *Surf. Sci.* **1975**, *48*, 549.